

Supplementary Information

Binary all-polymer solar cells with 19.30% efficiency enabled by bromodibenzothiophene-based solid additive

Haisheng Ma,^a Jiali Song,^b Jiawei Qiao,^c Bingyu Han,^d Qianqian Wang,^e Min Hun Jee,^f Laju Bu,^d

*Donghui Wei,^e Han Young Woo,^f Xiaotao Hao,^c Yanming Sun *^{a,b}*

^aHangzhou International Innovation Institute, Beihang University, Hangzhou 311115, P. R. China,

E-mail: sunym@buaa.edu.cn.

^bSchool of Chemistry, Beihang University, Beijing 100191, P. R. China, E-mail:

sunym@buaa.edu.cn.

^cSchool of Physics State Key Laboratory of Crystal Materials Shandong University Jinan 250100,

P. R. China.

^dSchool of Chemistry, Xi'an Jiaotong University, Xi'an, Shaanxi 710049, P. R. China.

^eCollege of Chemistry, Zhengzhou University, Zhengzhou, Henan 450001, P. R. China.

^fDepartment of Chemistry, College of Science, KU-KIST Graduate School of Converging Science

and Technology, Korea University, Seoul 136-713, Republic of Korea.

Materials and Reagents

PM6, PY-DT¹, PY-IT² and PY-C11³ were purchased from Solarmer Materials (Beijing, China). Chloroform (CF) was purchased from Sigma Aldrich. DBTP and 4-BDBTP were purchased from Macklin (Shanghai, China).

Device fabrication

All-polymer solar cells (all-PSCs) were fabricated with a device structure of ITO/2PACz/PM6:polymer acceptors/PNDIT-F3N/Ag. The ITO-coated substrates were cleaned by detergent deionized water, acetone, and isopropyl alcohol for 15 min each in ultrasonic cleaning machine sequentially. The cleaned ITO-coated substrates were dried in an oven at 100 °C overnight. Before used, the ITO-coated substrates were pretreated by a plasma cleaner for 2 min under a vacuum condition of 10 Pa. 2PACz was adequately dissolved in ethanol at a concentration of 0.3 mg/ml, after which the solution was spin-coated on top of the ITO substrates at 3000 rpm for 30 s and then thermal annealed at 100 °C for 10 min under nitrogen conditions. The active layers were generated by spin-coating active layer solution on the top of 2PACz layer for 30 s at a rate of 2500 rpm with an optimal thickness of 110 nm under nitrogen atmosphere. The D:A weight ratios of CF solution was 1:1. The total concentration of CF solution was 12.5 mg/ml. The optimal weight ratios of DBTP and 4-BDBTP to the total mass of PM6 acceptor were 200% and 150%, respectively. The CF solutions were stirred at normal temperature (25 °C) for 4 hours before used. The corresponding blends were generated by spin coating the solutions on the PEDOT layer. Then, the active layers were all thermal annealing at 80 °C for 7 min. Subsequently, a PNDIT-F3N layer with a concentration of 1.2 mg/ml in mixed solvent (methanol: acetic acid is 500:1 by volume) was spin coated onto the active layer at a rate of 4200 rpm for 30 s. Finally, 120 nm Ag electrode

were deposited under a vacuum condition of 4×10^{-4} Pa. The active area of devices is 5.12 mm².

The devices were tested through a mask with an area of 3.15 mm².

Device characterizations

Device performance was measured by using a 510 Air Mass 1.5 Global (AM1.5G) solar simulator (SS-F5-3A, Enlitech) with an irradiation intensity of 100 mW cm⁻², which was determined using a calibrated silicon solar cell (SRC2020, Enlitech). The *J-V* curves were measured from -0.5 to 1 V with a scan step of 50 mV and a dwell time of 10 ms, along the forward scan direction, using a Keithley 2400 Source Measure Unit. EQE spectra were obtained by using a QE-R3011 Solar Cell EQE measurement system (Enlitech). UV-vis absorption spectra were performed by using a Shimadzu (model UV-3700) UV-vis spectrophotometer. SCLC measurements were adopted to examine charge mobilities of the blend by using hole-only devices with a structure of ITO/PEDOT:PSS/active layer/MoO₃/Ag, electron-only devices with a structure of ITO/ZnO/active layer /PNDIT-F3N/Ag under dark condition. The mobilities were determined by fitting corresponding *J-V* characteristics according to the Mott-Gurney law: $J = (9/8)\epsilon_r\epsilon_0\mu(V^2/L^3)$, in which J is the current density, ϵ_r is the dielectric permittivity of the transport medium, ϵ_0 is the vacuum permittivity of free space, L is the thickness of the active layer, and μ is the mobility. $V = V_{app} - V_{bi} - V_r$, where V_{app} is the applied voltage, V_{bi} is the offset voltage, and V_r is the voltage loss on series resistance. GIWAXS measurements were carried out at the PLS-II 9A U-SAXS beamline of the Pohang Accelerator Laboratory in Korea. AFM measurements were performed by Dimension Icon AFM (Bruker) in a tapping mode.

Computational details

All computations were performed with the Gaussian 09⁴ program by using density functional theory (DFT). Then, the geometry optimization of compounds was carried out with the M06-2X⁵ functional using 6-31G (d, p) basis set.⁶

Transient photocurrent (TPC) measurements

TPC of the devices were measured by applying a 488 nm solid state laser (Coherent OBIS CORE 488LS) with a pulse width of ~30 ns. The current traces were recorded using a mixed domain oscilloscope (Tektronix MDO3032) by measuring the voltage drop across a 2 Ω resistor load connected in series with the devices.

Device encapsulation process

Use capillary tube to suck the encapsulation adhesive evenly and gently coated on the device surface, then use 1.6*0.8 glass pieces to cover the surface of the device, squeeze out the extra air bubbles, then irradiate under the UV lamp for 2 minutes to solidify the encapsulation adhesive, then thermal stability and photostability characterization can be carried out.

Device photostability characterizations

The photostability data of the devices was measured by using Maximum Power Point (MPP) tracking mode (YH-VMPP-IV-16). The decay curves of these encapsulated devices were measured under continuous LED light source (380-810 nm, one solar intensity) in ambient air conditions (the average humidity was 20%, the average tested temperature was 25 °C). The device encapsulation procedure is shown as follow: Firstly, a layer of UV-curable adhesive was evenly smeared on the electrode surface of device in the N₂ atmosphere. Then, a piece of coverslip was put on the top of adhesive. Finally, the device was illuminated under UV light source (365 nm) for 3 minutes.

In-situ absorption measurements

The in-situ absorption measurements were detected by Spectrum Microvision DU-200. The detection range of the instrument is 186-1026 nm with a spectral resolution of 0.01 nm and a time resolution of 1 ms.

Transient absorption spectroscopy measurements

Femtosecond transient absorption spectroscopy measurements were performed on an Ultrafast Helios pump-probe system in collaboration with a regenerative amplified laser system from Coherent. An 800 nm pulse with a repetition rate of 1kHz, a length of 100 fs, and an energy of 7 mJ/pulse, was generated by an Ti:sapphire amplifier (Astrella, Coherent). The time delay between pump and probe was controlled by a motorized optical delay line with a maximum delay time of 8 ns. The samples films were spin-coated onto the 1 mm-thick quartz plates and are encapsulated by epoxy resin in nitrogen-filled glove box to resist water and oxygen in the air. The pump pulse is chopped by a mechanical chopper with 500 Hz and then focused on to the mounted sample with probe beams. The probe beam was collimated and focused into a fiber-coupled multichannel spectrometer with CCD sensor. The energy of pump pulse was measured and calibrated by a power meter (PM400, Thorlabs).

Figures and Tables

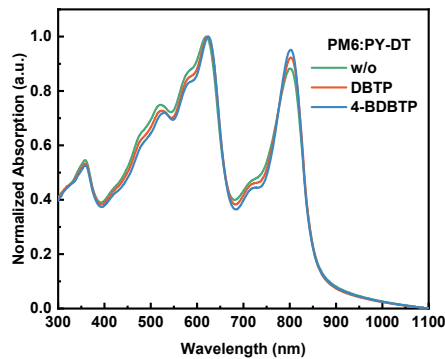


Fig. S1. Normalized absorption spectra of PM6:PY-DT blends processed under different conditions.

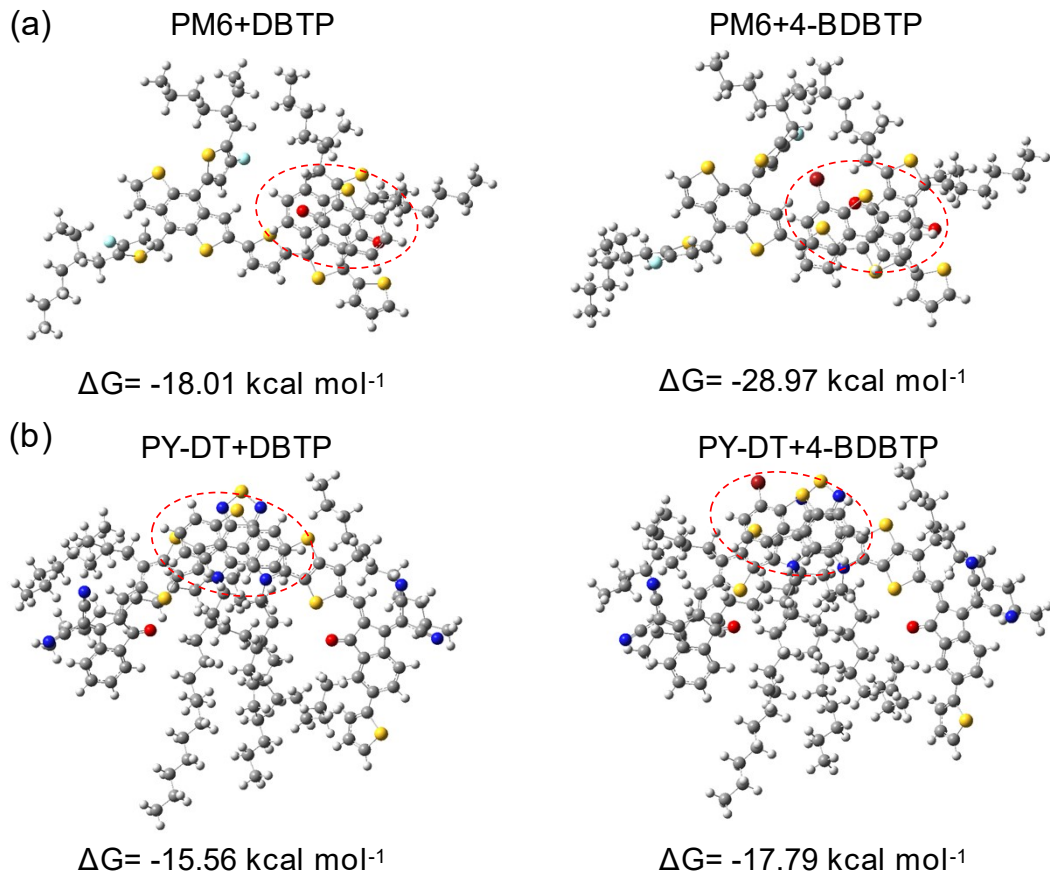


Fig. S2. The strongest conformations and calculated binding energies of the two additives with (a) PM6 and (b) PY-DT.

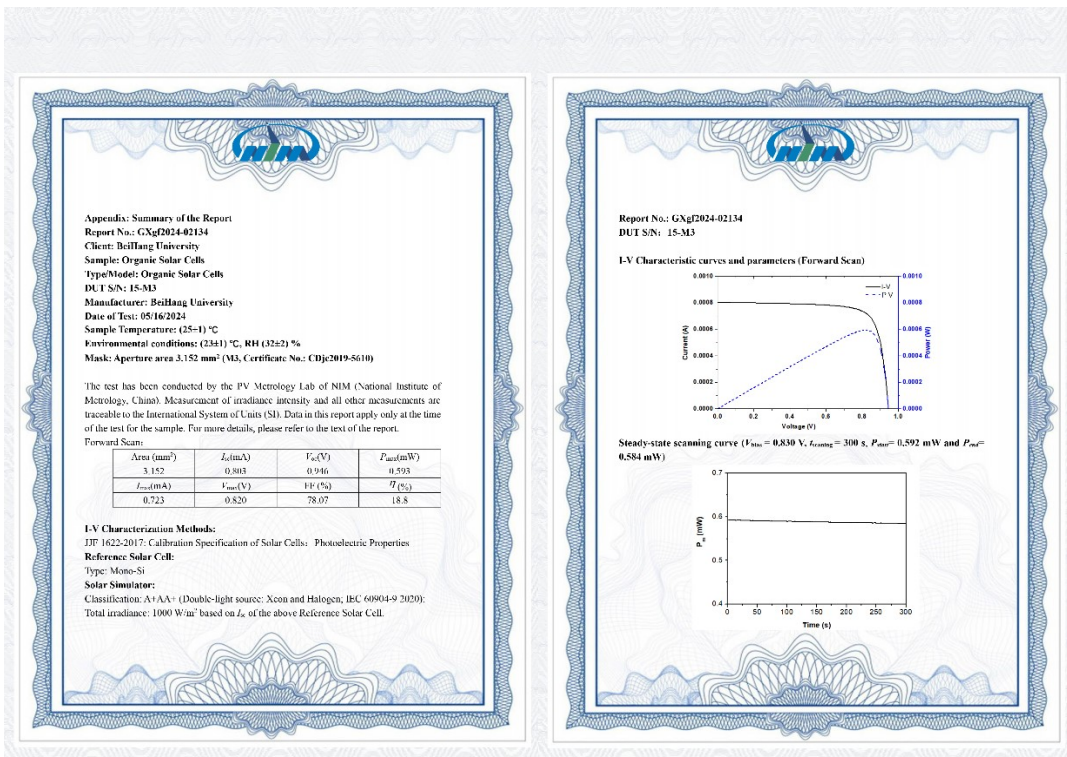


Fig. S3. The certification report of PM6:PY-DT device processed with 4-BDBTP from National Institute of Metrology (NIM), China.

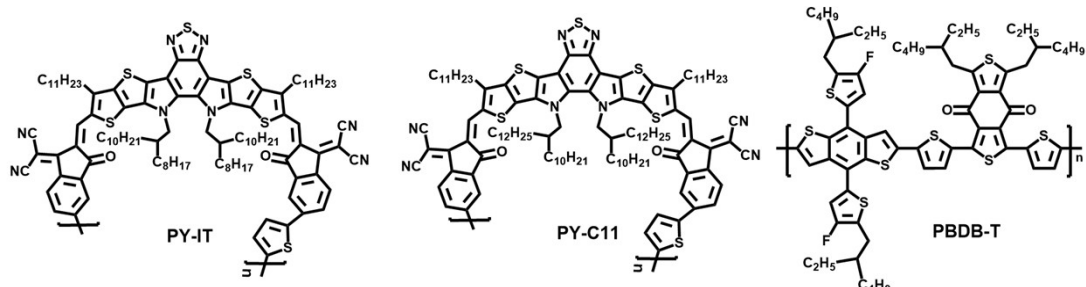


Fig. S4. Chemical structures of PY-IT, PY-C11 and PBDB-T.

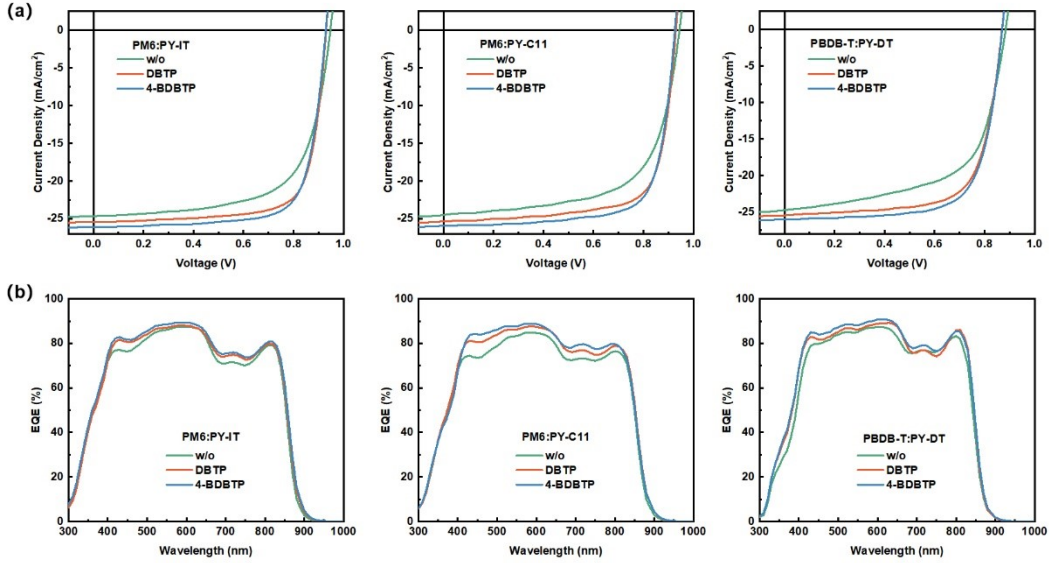


Fig. S5. (a) J - V characteristics and (b) the corresponding EQE spectra of PM6:PY-IT, PM6:PY-C11 and PBDB-T:PY-DT devices processed under different conditions.

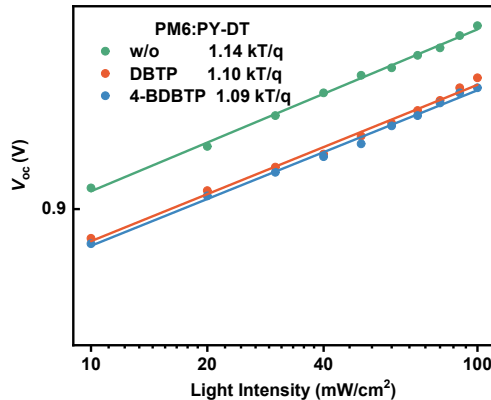


Fig. S6 V_{oc} versus light intensity characteristics of all-PSCs with different treatments.

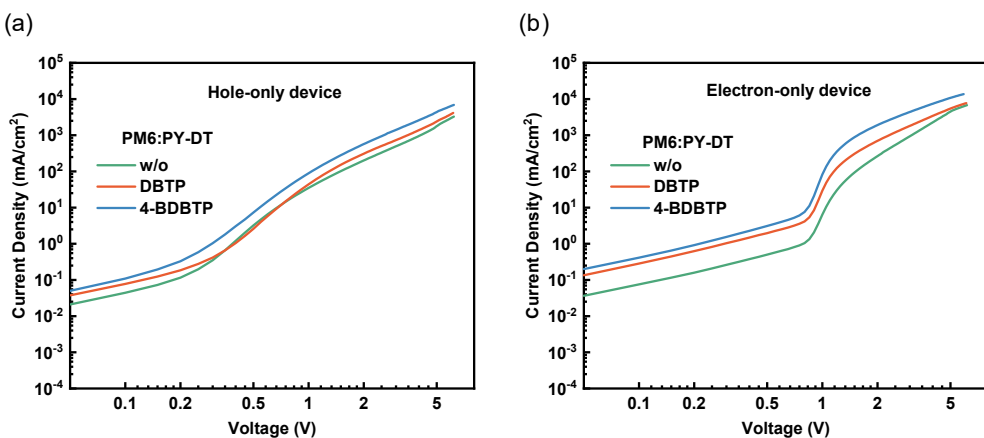


Fig. S7 SCLC curves of (a) hole-only devices and (b) electron-only devices treated under different conditions.

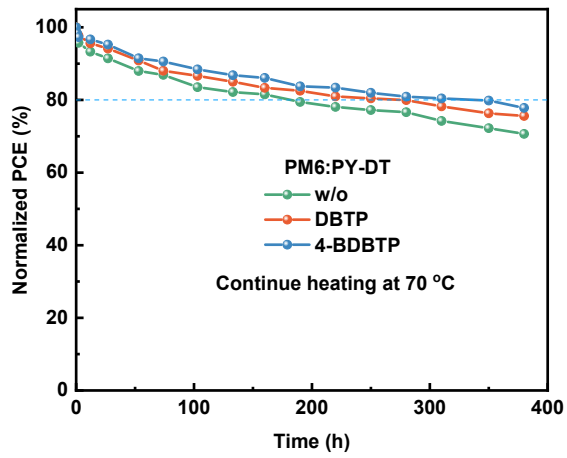


Fig. S8 Normalized PCE degradation lines of all-PSCs processed under different conditions stored under continuous heating at 70 °C.

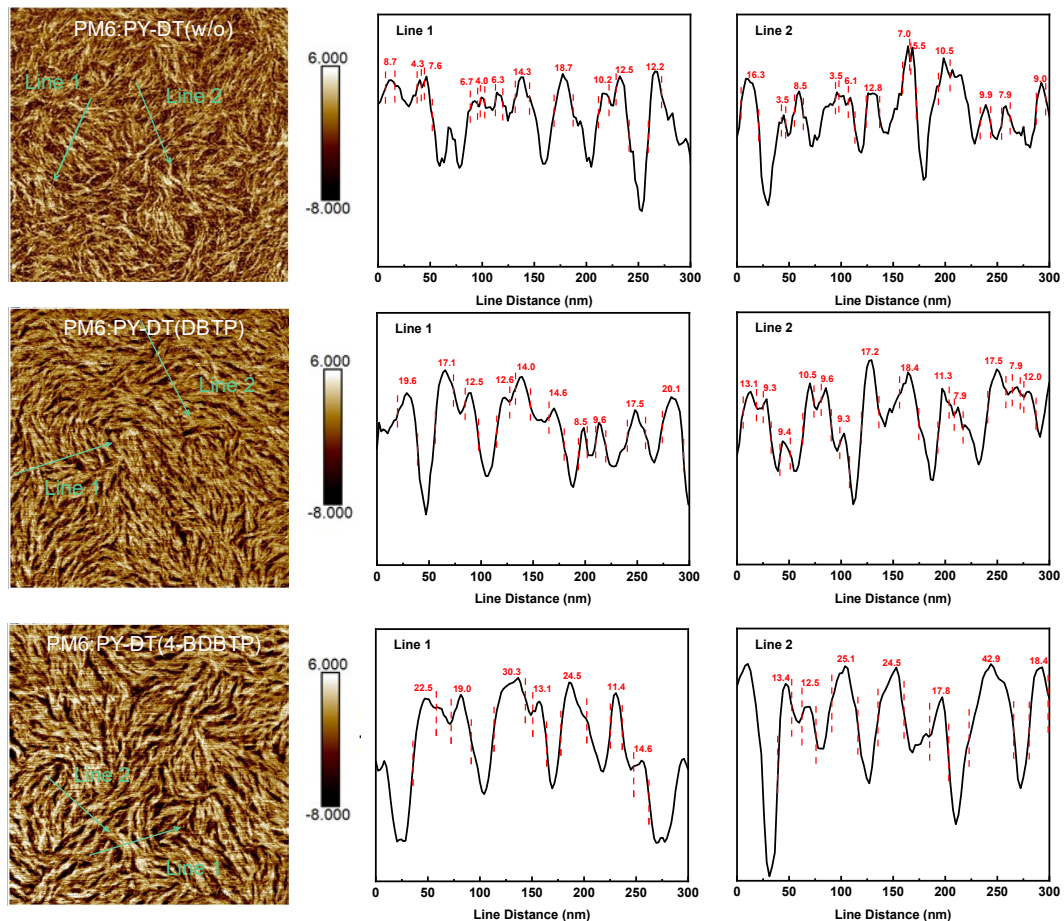


Fig. S9 Phase images and corresponding line-cut profiles of PM6:PY-DT blends processed under different conditions.

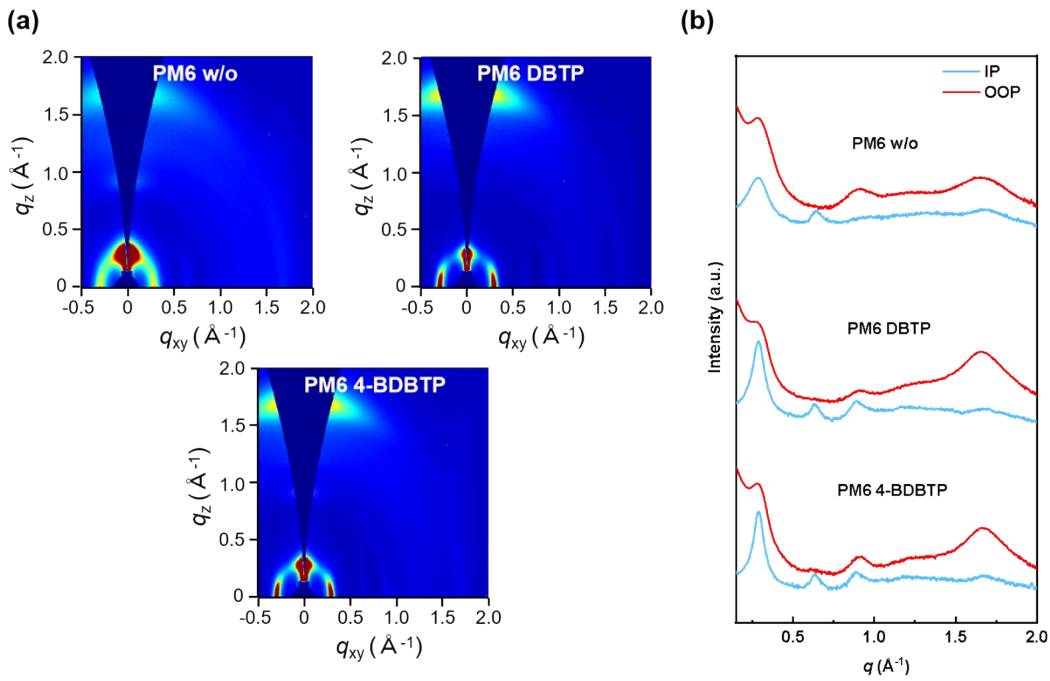


Fig. S10 (a) 2D GIWAXS patterns and (b) the corresponding out-of-plane and in-plane line cuts of the PM6 neat films processed under different conditions.

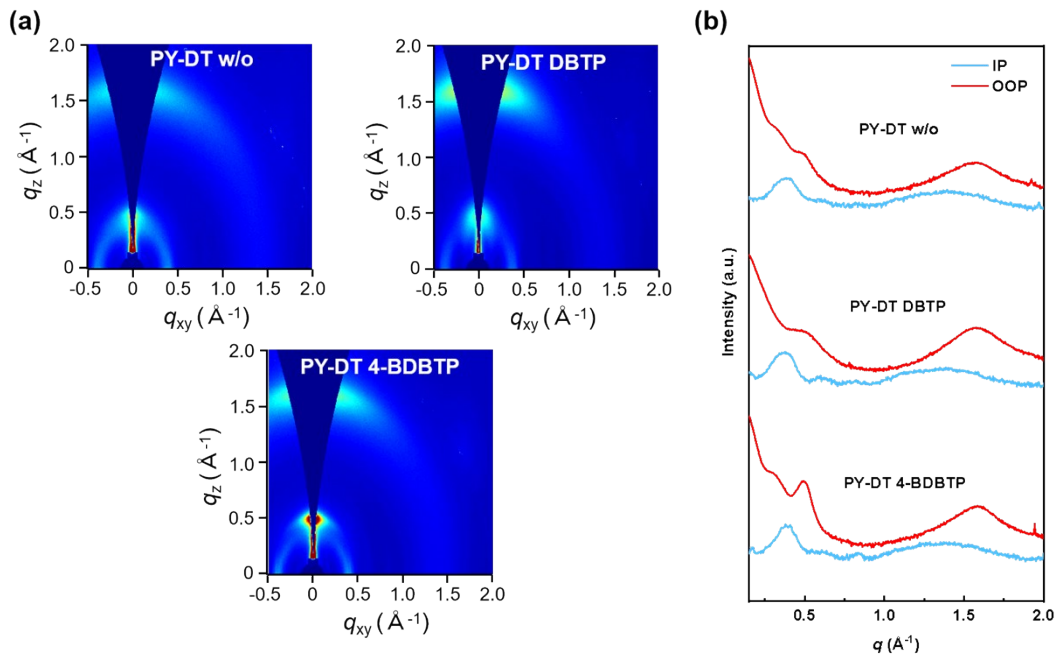


Fig. S11 (a) 2D GIWAXS patterns and (b) the corresponding out-of-plane and in-plane line cuts of the PY-DT neat films processed under different conditions.

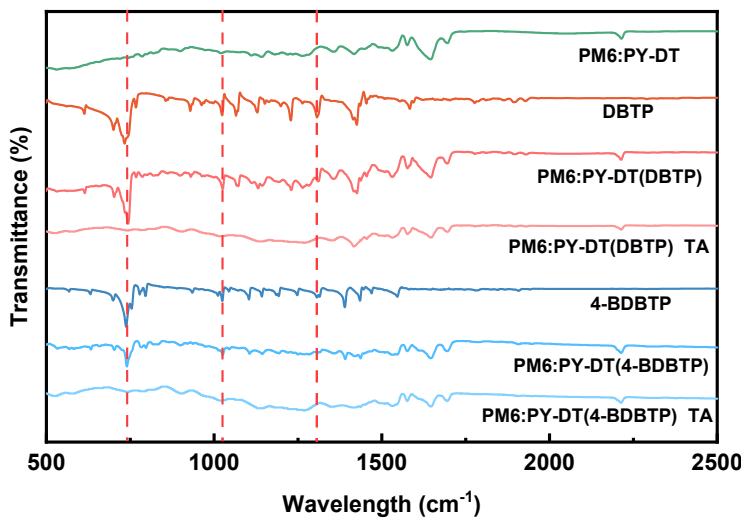


Fig. S12 FT-IR spectra of PM6:PY-DT, DBTP, and PM6:PY-DT blends treated with DBTP and 4-BDBTP before and after thermal annealing.



Fig. S13 Volatilization process of DBTP and 4-BDBTP on silicon substrate heated at 80 °C.

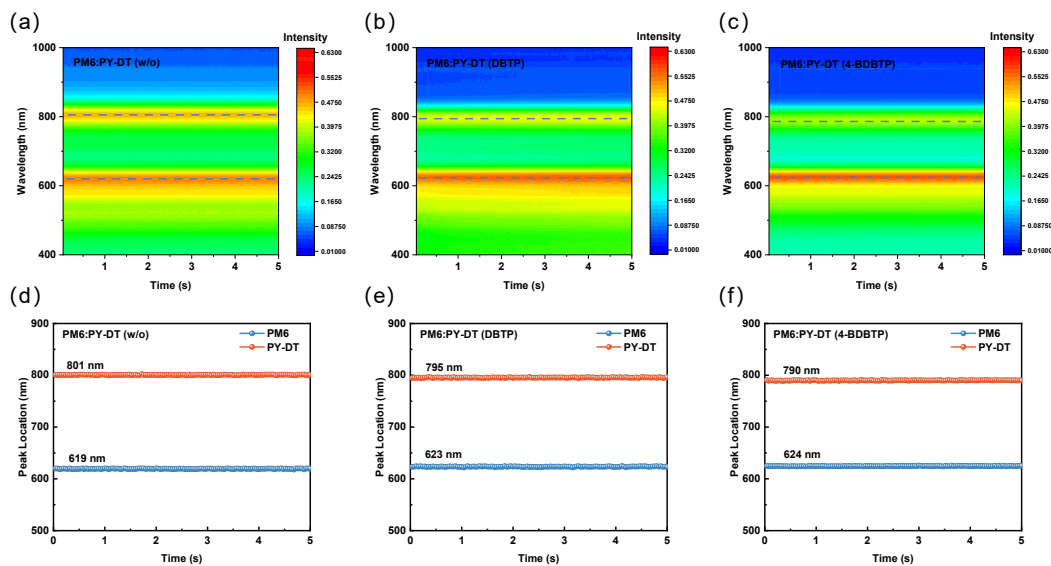


Fig. S14 (a-c) In situ 2D UV-Visible absorption of PM6:PY-DT blend treated under different conditions during spin coating process. (d-f) The time evolution of the peak location of PM6 and PY-DT in the blend treated under different conditions during spin coating process.

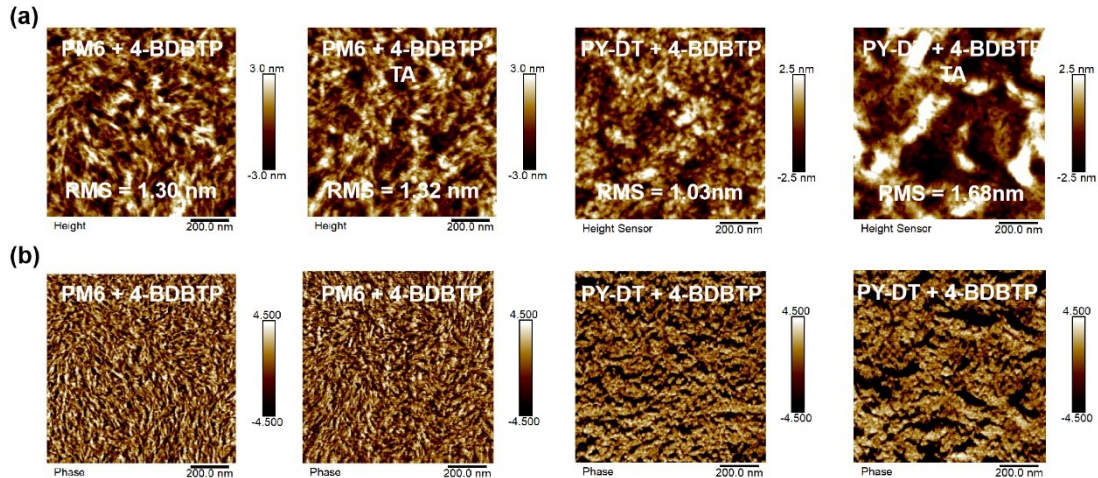


Fig. S15 AFM (a) height images and (b) phase images of 4-BDBTP-processed PM6 and PY-DT neat films before and after thermal annealing.

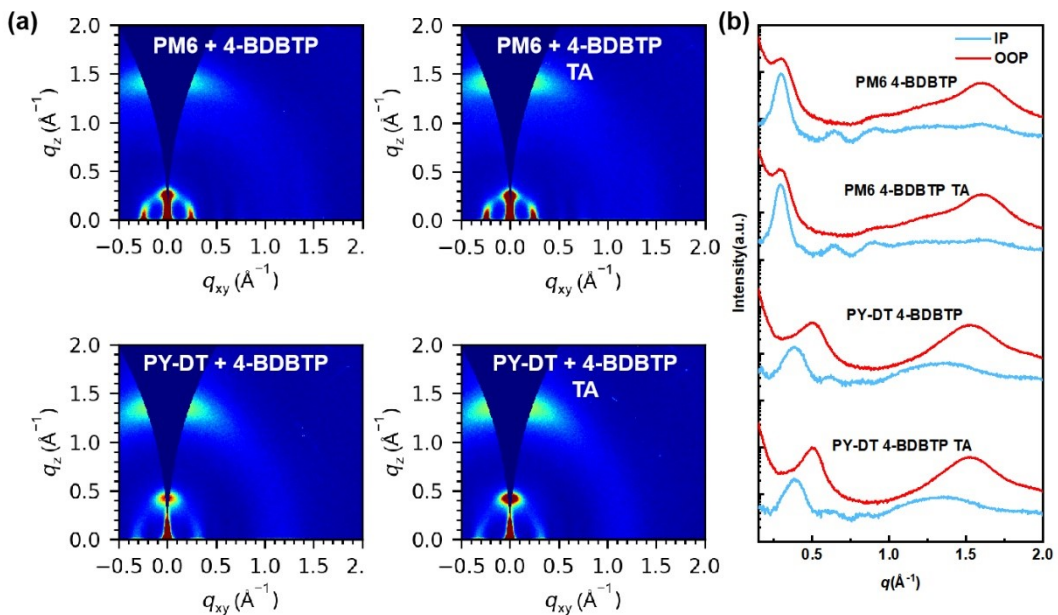


Fig. S16 (a) 2D GIWAXS patterns and (b) the corresponding in-plane and out-of-plane line-cuts of 4-BDBTP-processed PM6 and PY-DT neat films before and after thermal annealing.

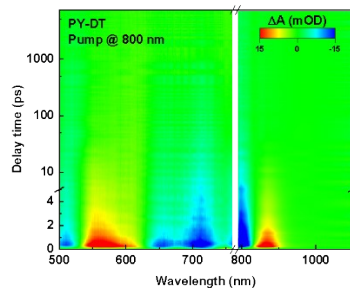


Fig. S17 2D TAS images of PY-DT films with 800 nm excitation.

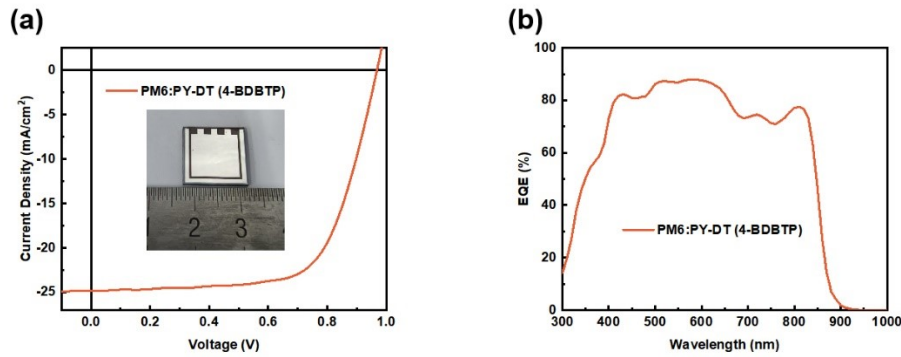


Fig. S18 (a) J - V characteristics and (b) the corresponding EQE spectra of the large-area PM6:PY-DT all-PSC (1 cm^2) processed with 4-BDBTP.

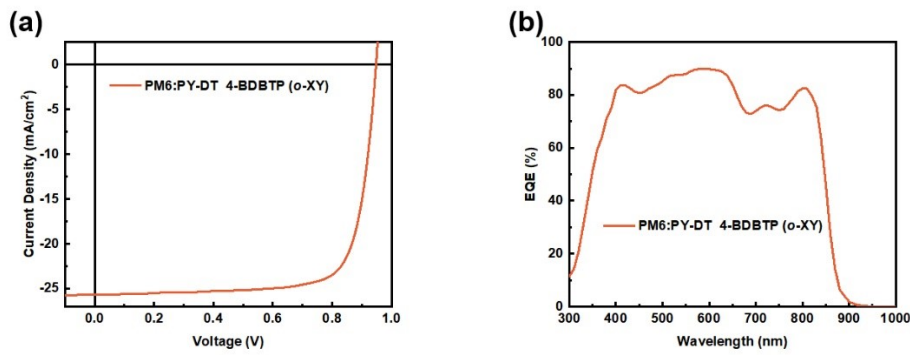


Fig. S19 (a) J - V characteristics and (b) the corresponding EQE spectra of *o*-XY-processed PM6:PY-DT device with 4-BDBTP.

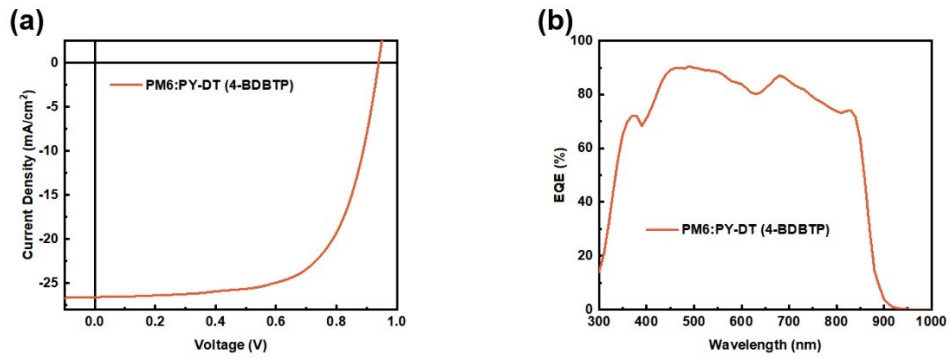


Fig. S20 (a) J - V characteristics and (b) the corresponding EQE spectra of PM6:PY-DT thick-film (300nm) device with 4-BDBTP.

Table S1. Detailed photovoltaic parameters of the PM6:PY-DT based devices processed under various conditions. The weight ratio of PM6 and PY-DT was 1:1.

Additive	w%	TA	V_{oc}	J_{sc}	FF	PCE
	(%)	(°C)	(V)	(mA cm ⁻²)	(%)	(%)
DBTP	100	80	0.954	24.32	74.7	17.33
		60	0.954	24.55	75.2	17.61
	200	80	0.952	25.21	76.5	18.36
		100	0.951	24.73	76.1	17.90
4-BDBTP	300	80	0.952	24.48	75.5	17.60
		80	0.955	24.16	74.3	17.14
	100	80	0.954	24.75	75.7	17.87
		60	0.952	25.36	74.7	18.03
4-BDBTP	150	80	0.951	25.85	78.5	19.30
		100	0.949	25.32	77.7	18.67
	200	80	0.952	24.73	77.9	18.34
	300	80	0.950	23.70	76.0	17.11

Table S2. Summarized photovoltaic parameters for the all-PSCs.

Active layer	V_{oc}	J_{sc}	FF	PCE	Reference
	(V)	(mA cm ⁻²)	(%)	(%)	
Binary all-polymer solar cells					
PM6:PY-82	0.950	23.82	75.80	17.15	3
PM6:PY2F-T	0.887	26.20	74.80	17.38	7
PM6:PYDT-3F	0.923	24.49	77.01	17.41	8
PM6:PZC17	0.929	22.70	71.79	15.14	9
PM6:PY-DF	0.970	23.10	70.20	15.70	10
PM6:SH-1	0.979	21.03	68.67	14.14	11
PM6:PY-V- γ	0.912	24.80	75.80	17.10	12
PBDB-T:PY-Se	0.891	23.52	73.85	15.48	13

PBDB-T:PYT-Tz	0.916	23.00	71.68	15.10	14
PM6:PT-YTz	0.871	26.27	70.59	16.15	15
PM6:PG-IT2F	0.950	24.03	75.46	17.24	16
PM6:PY-IT	0.933	25.61	76.50	18.30	17
PM6:PY-DT	0.951	23.84	76.40	17.32	18
PM6:PY-DT	0.949	23.73	74.40	16.76	19
PBDB-T:PYFS-Reg	0.920	23.52	74.00	16.09	20
PBDB-T:PTIC-HD-4Cl	0.834	23.84	68.98	13.71	21
PM6:PYF-V- <i>o</i>	0.884	25.10	73.70	16.40	22
PBDB-T:PZT-C1	0.912	23.90	68.50	14.90	23
PBQ6:PYF-T- <i>o</i>	0.886	25.12	76.64	17.06	24
PM6:PY2Se-Cl	0.884	24.50	74.30	16.10	25
PBDB-T:PJ1	0.900	23.10	77.30	16.10	26
PM6:PA1- <i>o</i>	0.925	23.99	72.20	16.00	27
JD40:PA-5	0.870	24.05	76.88	16.11	28
PM6:PYT1	0.938	21.50	66.66	13.43	29
PM6:PY-IT	0.945	26.37	76.48	19.06	30
PM6:PY-V- γ	0.913	24.90	77.70	17.70	31
PQM-Cl:PY-IT	0.920	24.30	80.70	18.00	32
PQB-2:PY-IT	0.942	24.20	79.50	18.10	33
PM6:L15	0.930	25.95	77.26	18.72	34
PM6:PY-C11	0.937	24.92	78.60	18.35	35
PBQx-TCl:PYIT2	0.938	24.61	79.66	18.39	36
PM6:PY-DT-X	0.953	25.87	79.10	19.50	37
PM6:PY-NFT	0.940	25.94	78.40	19.12	38
PM6:PY-DT	0.951	25.85	78.50	19.30	This work
Ternary all-polymer solar cell					
PM6:PY-SSe-V:PY-Cl	0.910	25.88	77.04	18.14	39
PM6:PYT-1S1Se:PYT-1S1Se-4Cl	0.902	25.50	77.12	17.74	40

PM6:PY-1S1Se:PY-2Cl	0.914	25.74	77.20	18.20	41
PM6:PY-DT:PYF-T-o	0.946	24.57	78.10	18.15	42
PM6:PY-V- γ :PJ1- γ	0.940	25.50	75.30	18.10	43
PBQx-TF:PBDB-TF:PY-IT	0.931	24.50	79.60	18.20	44
PM6:PY-82:PY-DT	0.947	24.31	78.30	18.03	45
PBQx-TCl:PY-IT:PY-IV	0.943	25.25	79.00	18.81	46
PM6:PY-V- γ :PFBO-C12	0.905	25.80	77.00	18.00	47
PQM-Cl:PTQ10:PY-IT	0.943	24.80	78.90	18.45	48
PBBTz-Cl:PY-IT:BTP-2T2F	0.922	25.82	78.11	18.60	49
PM6:PY-IT: PYFCl-T	0.940	25.76	74.84	18.12	50
PM6:PY-IT:PPCBMB	0.956	24.16	78.10	18.04	51
PM6:PY-DT:Y6	0.945	24.51	77.80	18.02	52
PDBQx-TCl:PY-IT:BTA3-4F	0.934	24.90	79.80	18.60	53
PM6:PBQx-TCl:PY-IT	0.954	25.47	78.19	19.00	54
PM6:PQx3:PYF-T-o	0.934	25.54	78.88	18.82	55
QQ1:PY-IT:F-BTA3	0.917	26.59	78.75	19.20	56
PBDB-TFCl:D18-Cl:PY-IT	0.958	24.50	79.30	18.60	57
PM6 :PY-DT: L8-BO	0.961	26.50	74.50	19.02	58
PM6:PY-V- γ : PffBQx-T	0.917	26.00	78.40	18.70	59

Table S3. Detailed photovoltaic parameters of PM6:PY-IT, PM6:PY-C11 and PBDB-T:PY-DT devices processed under different conditions.

Active layer	Condition	V_{oc} (V)	J_{sc} (mA/cm ²)	FF (%)	PCE (%)
PM6:PY-IT	w/o	0.951	24.62	66.2	15.50
	DBTP	0.932	25.43	76.2	18.06
	4-BDBTP	0.930	26.05	77.0	18.65
	w/o	0.947	24.50	65.1	14.67
PM6:PY-C11	DBTP	0.931	25.33	75.8	17.88

	4-BDBTP	0.927	25.93	76.6	18.41
	w/o	0.884	24.73	64.2	14.03
PBDB-T:PY-DT	DBTP	0.871	25.48	75.3	16.71
	4-BDBTP	0.871	25.96	76.8	17.37

Table S4. Charge mobilities of PM6:PY-DT blends processed under different conditions.

Blend	μ_h ($10^{-4} \text{ cm}^2 \text{ V}^{-1} \text{ s}^{-1}$)	μ_e ($10^{-4} \text{ cm}^2 \text{ V}^{-1} \text{ s}^{-1}$)	μ_e/μ_h
PM6:PY-DT (w/o)	3.87	6.09	1.57
PM6:PY-DT (DBTP)	4.70	7.26	1.55
PM6:PY-DT (4-BDBTP)	6.23	8.06	1.29

Table S5. Crystal coherence length and the d spacing of (100) peaks in IP direction and (010) peaks in OOP direction of PM6, PY-DT neat films and PM6:PY-DT blends processed under different conditions.

Film	100 (IP)				010 (OOP)			
	q (\AA^{-1})	d -spacing (\AA)	FWHM (\AA^{-1})	CCL (\AA)	q (\AA^{-1})	d -spacing (\AA)	FWHM (\AA^{-1})	CCL (\AA)
PM6 (w/o)	0.283	22.20	0.083	67.37	1.649	3.81	0.287	19.48
PM6 (DBTP)	0.287	21.89	0.044	127.09	1.659	3.79	0.186	30.06
PM6 (4-BDBTP)	0.288	21.82	0.038	147.16	1.669	3.76	0.177	31.59
PY-DT (w/o)	0.366	17.17	0.166	33.69	1.560	4.03	0.270	20.71
PY-DT (DBTP)	0.378	16.62	0.148	37.78	1.575	3.99	0.239	23.40
PY-DT (4-BDBTP)	0.385	16.32	0.100	55.92	1.578	3.98	0.226	24.74
PM6:PY-DT (w/o)	0.293	21.44	0.118	47.39	1.607	3.91	0.305	18.33
PM6:PY-DT (DBTP)	0.295	21.30	0.067	83.46	1.618	3.88	0.253	22.10
PM6:PY-DT (4-BDBTP)	0.298	21.08	0.063	88.76	1.628	3.86	0.232	24.10

Table S6. Crystal coherence length and the d spacing of (100) peaks in IP direction and (010) peaks in OOP direction of PM6, PY-DT neat films processed with 4-BDBTP before and after thermal annealing.

Film	100 (IP)				010 (OOP)			
	<i>q</i>	<i>d</i> -spacing	FWHM	CCL	<i>q</i>	<i>d</i> -spacing	FWHM	CCL
	(Å ⁻¹)	(Å)	(Å ⁻¹)	(Å)	(Å ⁻¹)	(Å)	(Å ⁻¹)	(Å)
PM6 4-BDBTP	0.295	21.30	0.061	91.67	1.6	3.93	0.218	25.65
PM6 4-BDBTP TA	0.295	21.30	0.059	94.78	1.603	3.92	0.209	26.76
PY-DT 4-BDBTP	0.381	16.49	0.134	41.73	1.523	4.13	0.25	22.37
PY-DT 4-BDBTP TA	0.384	16.36	0.105	53.26	1.525	4.12	0.247	22.64

Table S7. Fitted parameters for TA kinetics at PY-DT GSB (Pump @ 800 nm) of blends treated under different conditions.

Blend	τ_1	τ_2
PM6:PY-DT(w/o)	1.54	16.37
PM6:PY-DT(DBTP)	0.66	13.29
PM6:PY-DT(4-BDBTP)	0.51	7.60

Table S8. Detailed photovoltaic parameters of the large-area PM6:PY-DT all-PSC (1 cm²) processed with 4-BDBTP.

Active layer	<i>V</i> _{oc} (V)	<i>J</i> _{sc} (mA/cm ²)	FF (%)	PCE ^a (%)
PM6:PY-DT	0.968	24.85	71.8	17.27
(4-BDBTP)	(0.966 ± 0.03)	(24.65 ± 0.36)	(70.6 ± 1.5)	(17.02 ± 0.25)

^a Average value obtained from 10 independent devices.

Table S9. Detailed photovoltaic parameters of *o*-XY-processed PM6:PY-DT device with 4-BDBTP.

Active layer	V_{oc} (V)	J_{sc} (mA/cm ²)	FF (%)	PCE ^a (%)
PM6:PY-DT	0.952	25.66	78.0	19.07
(4-BDBTP)	(0.951 ± 0.02)	(25.47 ± 0.28)	(77.5 ± 0.8)	(18.93 ± 0.14)

^a Average values obtained from 10 devices.

Table S10. Detailed photovoltaic parameters of PM6:PY-DT thick-film (300nm) device with 4-BDBTP.

Active layer	V_{oc} (V)	J_{sc} (mA/cm ²)	FF (%)	PCE ^a (%)
PM6:PY-DT	0.941	26.59	69.8	17.46
(4-BDBTP)	(0.939 ± 0.03)	(26.33 ± 0.30)	(68.9 ± 0.9)	(17.30 ± 0.16)

^a Average values obtained from 10 devices.

References

- Y. Li, J. Song, Y. Dong, H. Jin, J. Xin, S. Wang, Y. Cai, L. Jiang, W. Ma, Z. Tang and Y. Sun, *Adv. Mater.*, 2022, **34**, 2110155.
- Z. Luo, T. Liu, R. Ma, Y. Xiao, L. Zhan, G. Zhang, H. Sun, F. Ni, G. Chai, J. Wang, C. Zhong, Y. Zou, X. Guo, X. Lu, H. Chen, H. Yan and C. Yang, *Adv. Mater.*, 2020, **32**, 2005942.
- Y. Li, Q. Li, Y. Cai, H. Jin, J. Zhang, Z. Tang, C. Zhang, Z. Wei and Y. Sun, *Energy Environ. Sci.*, 2022, **15**, 3854-3861.
- G. W. T. M. J. Frisch, H. B. Schlegel, G. E. Scuseria, M. A. Robb, J. R. Cheeseman, G. Scalmani, V. Barone, B. Mennucci, G. A. Petersson, H. Nakatsuji, M. Caricato, X. Li, H. P. Hratchian, A. F. Izmaylov, J. Bloino, G. Zheng, J. L. Sonnenberg, M. Hada, M. Ehara, K. Toyota, R. Fukuda, J. Hasegawa, M. Ishida, T. Nakajima, Y. Honda, O. Kitao, H. Nakai, T. Vreven, J. A. Montgomery, Jr., J. E. Peralta, F. Ogliaro, M. Bearpark, J. J. Heyd, E. Brothers, K. N. Kudin, V. N. Staroverov, R. Kobayashi, J. Normand, K. Raghavachari, A. Rendell, J. C. Burant, S. S. Iyengar, J. Tomasi, M. Cossi, N. Rega, J. M. Millam, M. Klene, J. E. Knox, J. B. Cross, V. Bakken, C. Adamo, J. Jaramillo, R. Gomperts, R. E. Stratmann, O. Yazyev, A. J. Austin, R. Cammi, C. Pomelli, J. W. Ochterski, R. L. Martin, K. Morokuma, V. G. Zakrzewski, G. A. Voth, P. Salvador, J. J. Dannenberg, S. Dapprich, A. D. Daniels, O. Farkas, J. B. Foresman, J. V. Ortiz, J. Cioslowski, and D. J. Fox, Gaussian 09, Revision B.01, Gaussian, Inc., Wallingford CT, 2010.

5. Y. Zhao and D. G. Truhlar, *Theor. Chem. Acc.*, 2008, **120**, 215-241.
6. M. M. Franch, W. J. Pietro, W. J. Hehre, J. S. Binkley, M. S. Gordon, D. J. Defrees and J. A. Pople, *J. Chem. Phys.*, 1982, **77**, 3654-3665.
7. H. Yu, Y. Wang, X. Zou, H. Han, H. K. Kim, Z. Yao, Z. Wang, Y. Li, H. M. Ng and W. Zhou, *Adv. Funct. Mater.*, 2023, **33**, 2300712.
8. D. Zhou, C. Liao, S. Peng, X. Xu, Y. Guo, J. Xia, H. Meng, L. Yu, R. Li and Q. Peng, *Adv. Sci.*, 2022, **9**, 2202022.
9. Z. Zhang, Z. Li, P. Wang, H. Chen, K. Ma, Y. Zhang, T. Duan, C. Li, Z. Yao and B. Kan, *Adv. Funct. Mater.*, 2023, **33**, 2214248.
10. H. Xiao, J. Lv, M. Liu, X. Guo, X. Xia, X. Lu and M. Zhang, *J. Mater. Chem. A*, 2023, **11**, 5584-5592.
11. Y. Huang, X. Si, R. Wang, K. Ma, W. Shi, C. Jiang, Y. Lu, C. Li, X. Wan and Y. Chen, *J. Mater. Chem. A*, 2023, **11**, 14768-14775.
12. H. Yu, Y. Wang, H. K. Kim, X. Wu, Y. Li, Z. Yao, M. Pan, X. Zou, J. Zhang and S. Chen, *Adv. Mater.*, 2022, **34**, 2200361.
13. Q. Wu, W. Wang, Y. Wu, R. Sun, J. Guo, M. Shi and J. Min, *Natl. Sci. Rev.*, 2022, **9**, nwab151.
14. T. Wang, R. Sun, X.-R. Yang, Y. Wu, W. Wang, Q. Li, C.-F. Zhang and J. Min, *Chin. J. Polym. Sci.*, 2022, **40**, 877-888.
15. T. Wang, R. Sun, Y. Wu, W. Wang, M. Zhang and J. Min, *Chem. Mater.*, 2022, **34**, 9970-9981.
16. G. Sun, X. Jiang, X. Li, L. Meng, J. Zhang, S. Qin, X. Kong, J. Li, J. Xin, W. Ma and Y. Li, *Nat. Commun.*, 2022, **13**, 5267.
17. W. Feng, T. Chen, Y. Li, T. Duan, X. Jiang, C. Zhong, Y. Zhang, J. Yu, G. Lu, X. Wan, B. Kan and Y. Chen, *Angew. Chem. Int. Ed.*, 2024, **63**, e202316698.
18. J. Song, Y. Li, Y. Cai, R. Zhang, S. Wang, J. Xin, L. Han, D. Wei, W. Ma and F. Gao, *Matter*, 2022, **5**, 4047-4059.
19. Y. Li, J. Song, Y. Dong, H. Jin, J. Xin, S. Wang, Y. Cai, L. Jiang, W. Ma and Z. Tang, *Adv. Mater.*, 2022, **34**, 2110155.
20. J.-W. Lee, C. Sun, S.-W. Lee, G.-U. Kim, S. Li, C. Wang, T.-S. Kim, Y.-H. Kim and B. J. Kim, *Energy Environ. Sci.*, 2022, **15**, 4672-4685.
21. H. Lai, H. Chen, Y. Zhu, H. Wang, Y. Li and F. He, *Macromolecules*, 2022, **55**, 3353-3360.
22. H. K. Kim, H. Yu, M. Pan, X. Shi, H. Zhao, Z. Qi, W. Liu, W. Ma, H. Yan and S. Chen, *Adv. Sci.*, 2022, **9**, 2202223.
23. H. Fu, Y. Li, Z. Wu, F. R. Lin, H. Y. Woo and A. K. Y. Jen, *Macromol. Rapid Commun.*, 2022, **43**, 2200062.
24. K. Hu, C. Zhu, K. Ding, S. Qin, W. Lai, J. Du, J. Zhang, Z. Wei, X. Li and Z. Zhang, *Energy Environ. Sci.*, 2022, **15**, 4157-4166.
25. Q. Fan, H. Fu, Z. Luo, J. Oh, B. Fan, F. Lin, C. Yang and A. K.-Y. Jen, *Nano Energy*, 2022, **92**, 106718.
26. F.-Z. Cui, Z. Chen, J.-W. Qiao, P. Lu, X. Du, W. Qin, H. Yin and X.-T. Hao, *ACS Energy Lett.*, 2022, **7**, 3709-3717.
27. J. Du, K. Hu, C. Zhu, J. Zhang, Z. Zhang, Z. Wei, L. Meng and Y. Li, *Macromolecules*, 2022, **55**, 7481-7487.
28. J. Jia, Q. Huang, T. Jia, K. Zhang, J. Zhang, J. Miao, F. Huang and C. Yang, *Adv. Energy Mater.*, 2022, **12**, 2103193.

29. Q. Wu, W. Wang, T. Wang, R. Sun, J. Guo, Y. Wu, X. Jiao, C. J. Brabec, Y. Li and J. Min, *Sci. China Chem.*, 2020, **63**, 1449-1460.
30. R. Zeng, L. Zhu, M. Zhang, W. Zhong, G. Zhou, J. Zhuang, T. Hao, Z. Zhou, L. Zhou and N. Hartmann, *Nat. Commun.*, 2023, **14**, 4148.
31. Y. Wang, H. Yu, X. Wu, D. Zhao, S. Zhang, X. Zou, B. Li, D. Gao, Z. Li and X. Xia, *Adv. Energy Mater.*, 2022, **12**, 2202729.
32. J. Wang, Y. Cui, Y. Xu, K. Xian, P. Bi, Z. Chen, K. Zhou, L. Ma, T. Zhang and Y. Yang, *Adv. Mater.*, 2022, **34**, 2205009.
33. T. Zhang, Y. Xu, H. Yao, J. Zhang, P. Bi, Z. Chen, J. Wang, Y. Cui, L. Ma and K. Xian, *Energy Environ. Sci.*, 2023, **16**, 1581-1589.
34. B. Liu, W. Xu, R. Ma, J.-W. Lee, T. A. Dela Peña, W. Yang, B. Li, M. Li, J. Wu, Y. Wang, C. Zhang, J. Yang, J. Wang, S. Ning, Z. Wang, J. Li, H. Wang, G. Li, B. J. Kim, L. Niu, X. Guo and H. Sun, *Adv. Mater.*, 2023, **35**, 2308334.
35. J. Song, L. Ye, C. Liu, Y. Cai, C. Zhang, G. Yue, Y. Li, M. H. Jee, Y. Zhao, D. Wei, H. Y. Woo and Y. Sun, *Energy Environ. Sci.*, 2023, **16**, 5371-5380.
36. P. Bi, T. Zhang, Y. Cui, J. Wang, J. Qiao, K. Xian, X. W. Chua, Z. Chen, W. P. Goh, L. Ye, X. Hao, J. Hou and L. Yang, *Adv. Energy Mater.*, 2023, **13**, 2302252.
37. J. Song, C. Li, H. Ma, B. Han, Q. Wang, X. Wang, D. Wei, L. Bu, R. Yang, H. Yan and Y. Sun, *Adv. Mater.*, 2024, **36**, 2406922.
38. X. Zhang, H. Gao, Y. Kan, X. Wang, W. Zhang, K. Zhou, H. Xu, L. Ye, R. Yang, Y. Yang, X. Hao, Y. Sun and K. Gao, *Angew. Chem. Int. Ed.*, 2024, e202415583, doi.org/10.1002/anie.202415583.
39. X. Yang, R. Sun, Y. Wang, M. Chen, X. Xia, X. Lu, G. Lu and J. Min, *Adv. Mater.*, 2023, **35**, 2209350.
40. X. Wu, X. Yang, Y. Shao, Y. Gao, J. Wan, S. Ponomarenko, Y. Luponosov, R. Sun and J. Min, *Sol. RRL*, 2023, **7**, 2300064.
41. R. Sun, T. Wang, Q. Fan, M. Wu, X. Yang, X. Wu, Y. Yu, X. Xia, F. Cui and J. Wan, *Joule*, 2023, **7**, 221-237.
42. J. Song, C. Li, J. Qiao, C. Liu, Y. Cai, Y. Li, J. Gao, M. H. Jee, X. Hao and H. Y. Woo, *Matter*, 2023, **6**, 1542-1554.
43. C. Zhao, R. Ma, Y. Hou, L. Zhu, X. Zou, W. Xiong, H. Hu, L. Wang, H. Yu, Y. Wang, G. Zhang, J. Yi, L. Chen, D. Wu, T. Yang, G. Li, M. Qiu, H. Yan, S. Li and G. Zhang, *Adv. Energy Mater.*, 2023, **13**, 2300904.
44. L. Ma, Y. Cui, J. Zhang, K. Xian, Z. Chen, K. Zhou, T. Zhang, W. Wang, H. Yao, S. Zhang, X. Hao, L. Ye and J. Hou, *Adv. Mater.*, 2023, **35**, 2208926.
45. Y. Cai, C. Xie, Q. Li, C. Liu, J. Gao, M. H. Jee, J. Qiao, Y. Li, J. Song, X. Hao, H. Y. Woo, Z. Tang, Y. Zhou, C. Zhang, H. Huang and Y. Sun, *Adv. Mater.*, 2023, **35**, 2208165.
46. R. Ma, H. Li, T. A. Dela Peña, X. Xie, P. W. K. Fong, Q. Wei, C. Yan, J. Wu, P. Cheng and M. Li, *Adv. Mater.*, 2024, **36**, 2304632.
47. H. Yu, Y. Wang, X. Zou, J. Yin, X. Shi, Y. Li, H. Zhao, L. Wang, H. M. Ng and B. Zou, *Nat. Commun.*, 2023, **14**, 2323.
48. R. Ma, Q. Fan, T. A. Dela Peña, B. Wu, H. Liu, Q. Wu, Q. Wei, J. Wu, X. Lu and M. Li, *Adv. Mater.*, 2023, **35**, 2212275.
49. P. Wu, Y. Duan, Y. Li, X. Xu, R. Li, L. Yu and Q. Peng, *Adv. Mater.*, 2024, **36**, 2306990.
50. J. Guo, X. Xia, B. Qiu, J. Zhang, S. Qin, X. Li, W. Lai, X. Lu, L. Meng and Z. Zhang, *Adv. Mater.*,

2023, **35**, 2211296.

51. T. Liu, K. Zhou, R. Ma, L. Zhang, C. Huang, Z. Luo, H. Zhu, S. Yao, C. Yang, B. Zou and L. Ye, *Aggregate*, 2023, **4**, e308.
52. Z. Ge, J. Qiao, Y. Li, J. Song, C. Zhang, Z. Fu, M. H. Jee, X. Hao, H. Y. Woo and Y. Sun, *Adv. Mater.*, 2023, **35**, 2301906.
53. Y. Xu, J. Wang, T. Zhang, Z. Chen, K. Xian, Z. Li, Y.-H. Luo, L. Ye, X. Hao and H. Yao, *Energy Environ. Sci.*, 2023, **16**, 5863-5870.
54. T. Chen, X. Zheng, D. Wang, Y. Zhu, Y. Ouyang, J. Xue, M. Wang, S. Wang, W. Ma, C. Zhang, Z. Ma, S. Li, L. Zuo and H. Chen, *Adv. Mater.*, 2024, **36**, 2308061.
55. D. Qiu, H. Zhang, C. Tian, J. Zhang, L. Zhu, Z. Wei and K. Lu, *Adv. Mater.*, 2023, **35**, 2307398.
56. Z. Wang, X. Wang, L. Tu, H. Wang, M. Du, T. Dai, Q. Guo, Y. Shi and E. Zhou, *Angew. Chem. Int. Ed.*, 2024, **63**, e202319755.
57. J. Wang, Y. Wang, K. Xian, J. Qiao, Z. Chen, P. Bi, T. Zhang, Z. Zheng, X. Hao and L. Ye, *Adv. Mater.*, 2024, **36**, 2305424.
58. T. Chen, Y. Zhong, T. Duan, X. Tang, W. Zhao, J. Wang, G. Lu, G. Long, J. Zhang, K. Han, X. Wan, B. Kan and Y. Chen, *Angew. Chem. Int. Ed.*, 2024, e202412983, doi.org/10.1002/anie.202412983.
59. H. Yu, Y. Wang, C. H. Kwok, R. Zhou, Z. Yao, S. Mukherjee, A. Sergeev, H. Hu, Y. Fu and H. M. Ng, *Joule*, 2024, **8**, 2304-2324.